JPhys Energy

TUTORIAL • OPEN ACCESS

In-operando characterization of energy materials using laboratory x-ray computed tomography

To cite this article: Krzysztof Dzieciol *et al* 2026 *J. Phys. Energy* **8** 023005

IOP Publishing J. Phys. Energy 8 (2026) 023005 https://doi.org/10.1088/2515-7655/ae7cb3

Journal of Physics: Energy

Check for updates

OPEN ACCESS

RECEIVED
29 January 2026

REVISED
1 June 2026

ACCEPTED FOR PUBLICATION
12 June 2026

PUBLISHED
25 June 2026

TUTORIAL

In-operando characterization of energy materials using laboratory x-ray computed tomography

Krzysztof Dzieciol[1,5,*], Sunghoon Choi[2,5], Luca Weckelmann[1,3], Rebecca Erkes[1,3], Rüdiger-A Eichel[1,3,4] and Florian Hausen[1]

[1] Institute of Energy Technologies, Fundamental Electrochemistry (IET-1), Forschungszentrum Jülich, D-52425 Jülich, Germany
[2] Electronics and Telecommunications Research Institute, Materials and Components Research Section, Gajeong-ro, Yuseong-gu, Daejeon 34129, Republic of Korea
[3] Institute of Physical Chemistry, RWTH Aachen University, D-52074 Aachen, Germany
[4] Faculty of Mechanical Engineering, RWTH Aachen University, D-52062 Aachen, Germany
[5] Contributed equally.
[*] Author to whom any correspondence should be addressed.

E-mail: k.dzieciol@fz-juelich.de

Keywords: XCT, tomography, in-operando, imaging

Abstract

In-operando laboratory x-ray computed tomography (XCT) enables non-destructive, real-time imaging of battery materials during electrochemical operation, providing critical insights into morphology evolution, degradation mechanisms, and performance limitations. This tutorial guides newcomers through the technique, emphasizing its role in battery research where dynamic processes like electrode plating, stripping, and phase transformations must be captured. Challenges such as optimizing temporal resolution versus image quality and reducing beam-induced damage are covered, with strategies like sparse sampling and super-resolution. Drawing on three examples—(1) hybrid 2D/3D imaging of zinc electrode evolution in various electrolytes Dzięcioł (2023); (2) high-frequency 3D *in-operando* study of anode morphology in a commercial zinc-air battery Dzięcioł (2025); and (3) a pressurized custom cell for air-sensitive lithium metal batteries Weckelmann (2025)—step-by-step instructions are provided. These instructions cover experiment design, execution, data handling, and practical tips. The tutorial stresses scripting for multi-modal synchronization, cell design for x-ray transparency, and artifact mitigation, equipping researchers to apply *in-operando* XCT effectively to various battery systems for innovative, sustainable solutions.

Glossary

In-operando: Latin for 'while operating,' referring to measurements conducted on a device or material under real working conditions, such as during battery charging/discharging.

In situ: Latin for 'in place,' describing experiments or measurements performed within the original environment or system, without removing the sample (e.g. imaging inside an electrochemical cell).

Ex situ: Latin for 'out of place,' referring to experiments or measurements conducted after removing the sample from its operational environment (e.g. post-mortem XCT after cycling).

Potentiostat: An electronic device that controls the voltage or current in an electrochemical cell to simulate battery operation.

Multi-modal imaging: The combination of two or more imaging techniques (e.g. 2D radiography + 3D XCT, or XCT + XRD) to provide complementary structural, chemical, or functional information in a single experiment.

FBP (filtered back-projection): A standard reconstruction algorithm that transforms projection data into a 3D volume using analytical filtering and back-projection; fast but sensitive to noise and undersampling.

FDK (Feldkamp-Davis-Kress): An extension of FBP for cone-beam geometry, widely used in laboratory XCT scanners for 3D reconstruction from circular trajectories.

ART (algebraic reconstruction technique): An iterative reconstruction method that solves a system of linear equations to minimize differences between measured and simulated projections; effective for sparse or noisy data.

TV (total variation): Regularization technique that minimizes the sum of the absolute gradients (spatial differences) of an image, promoting solutions that are piecewise smooth while preserving sharp boundaries.

U-Net: Convolutional neural network (CNN) architecture characterized by a U-shaped, symmetric encoder-decoder structure with skip connections, originally designed for precise, rapid image segmentation. It can be used also as image-to-image mapping tool to convert sparse-view, low-dose, or noisy raw XCT reconstructions into high-quality images.

Laminography: A tomographic technique for imaging flat or plate-like samples with limited rotation angles, reducing artifacts in large or constrained geometries; useful in battery pouch cells.

Sparse sampling: A method to reduce the number of x-ray projections needed for tomography, improving temporal resolution by reconstructing images from incomplete data sets.

Super-resolution: Techniques, often AI-based, to enhance image detail beyond the hardware's native resolution, useful for *in-operando* studies with limited scan time.

Beam damage: Alterations to sample structure caused by prolonged x-ray exposure, such as heating or chemical changes in sensitive materials.

Segmentation: The process of partitioning digital images into meaningful regions (e.g. electrode vs. electrolyte) for quantitative analysis.

Radiogram: A single 2D x-ray projection image

CNR: Contrast-to-noise ratio, a metric in imaging that measures how well an object can be distinguished from the background, calculated as the absolute difference in mean signal intensity between the object and background divided by the standard deviation of the noise.

4D imaging: four-dimensional imaging—refers to imaging techniques that capture three-dimensional spatial data over time, effectively adding time as the fourth dimension. This allows visualization of dynamic processes, such as motion, changes, or physiological activity in real-time or as a time-resolved sequence.

1. Introduction

In-operando x-ray computed tomography (XCT) in battery research allows nondestructive imaging of batteries while they operate, revealing real-time changes like electrode swelling or dendrite formation that static methods overlook [1]. This technique is particularly vital for understanding dynamic processes in emerging battery chemistries, where material evolution directly impacts safety, efficiency, and lifespan. For instance, in zinc-based systems, *in-operando* XCT can track plating and stripping, highlighting issues like shape change or passivation that hinder rechargeability [2, 3]. Similarly, in lithium metal batteries, it visualizes dendrite growth, a key failure mode [4]. Unlike synchrotron XCT, which requires specialized facilities, laboratory XCT remains accessible in standard labs but necessitates careful optimization for time and quality.

XCT basics are covered elsewhere [5, 6], but in short, a single experiment involves rotating a sample in an x-ray beam, capturing projections (2D images) at various angles, and reconstructing them into 3D volumes using algorithms like filtered back-projection (FBP or FDK for cone beam).

In *in-operando* studies, however, the classical paradigm of dense acquisition with analytical reconstruction is no longer sufficient. Laboratory *in-operando* XCT requires a balance among four competing requirements: spatial resolution, temporal resolution, signal quality, and radiation dose. Increasing magnification, exposure time, or projection number generally improves image quality and quantitative fidelity, but prolongs scans and may increase beam-induced perturbation. The practical role of sparse sampling, hybrid 2D/3D protocols, and super-resolution is therefore not to eliminate this trade-off, but to redistribute it in a controlled and application-dependent manner.

Recent work on ultrasparse-view tomography demonstrates that temporal resolution can be increased by orders of magnitude when acquisition and reconstruction are co-designed, using strong priors on image smoothness or dynamics [7]. Iterative, regularized algorithms such as TV minimization [8], implemented in modern toolboxes [9], allow robust reconstruction from heavily under-sampled data. Complementary super-resolution approaches exploit low-magnification, short-exposure scans together with high-quality training data, for instance from synchrotron XCT, to recover fine features in all-solid-state cells [10]. Hybrid schemes that interleave fast 2D radiography with intermittent 3D scans, or that employ laminography for flat pouch cells, further extend the design space by trading spatial for temporal resolution [11, 12].

The sample under investigation operates under external stimuli. These can be either an applied current or a mechanical force. The former is typical for battery systems. However, it is not uncommon to apply force or pressure—for example, in solid-state batteries. This requires additional hardware to control and measure the operating conditions on top of the imaging.

Since different systems require different components and bring system-specific challenges, this tutorial attempts to provide practical guidelines based on three studies addressing distinct aspects of *in-operando* imaging. Dzięcioł *et al.* [2], in fundamental research on a simplified symmetric cell, addresses the challenge of balancing 2D and 3D imaging techniques for real-time monitoring of morphology evolution. A more practical example from Dzięcioł *et al* [3] on a commercial battery, tackles the challenge of achieving high temporal resolution with fine 3D sampling to capture dynamic changes in anode morphology during *in-operando* conditions. Finally, Weckelmann *et al* [13] demonstrates the design of custom pressurized cells to manage the challenge of air-sensitive materials, ensuring stable imaging of lithium interfaces. All three cases, by combining XCT imaging with electrochemistry, facilitate multi-modal synchronization and data correlation, addressing the complexity of aligning structural and performance metrics to advance material and system development. As this is a short tutorial, the provided specifics will be limited. Readers are expected to dive into the corresponding references to learn more about, e.g. the choice of imaging parameters for a given study. Some basic knowledge of XCT and electrochemistry is required to fully benefit from this tutorial.

2. Design

Designing an *in-operando* laboratory XCT experiment for battery research begins by defining objectives, such as studying dendrite growth dynamics [2] or metal-air anode morphology changes [3]. This determines the setup and acquisition parameters. An essential component for electrochemical cycling is a potentiostat, typically connected via the scanner's access port. The required sensors, like a force sensor for stack pressure monitoring [13], are included based on specific requirements. Figure 1 shows common components of an *in-operando* imaging setup.

Electrochemical protocol mimics real operation while accommodating imaging windows. Scenarios, like high current to provoke dendritic versus smooth deposition, are simulated and validated against theoretical models such as Faraday's law. Protocols include rest periods to prevent motion artifacts or constant current for steady-state observation, and must align with imaging parameters including voltage, exposure time, projections, resolution, and modality. As a practical rule, slowly evolving, high-contrast morphologies can often be addressed with denser angular sampling and analytical reconstruction, whereas subtle interfacial features or faster dynamics may require sparse-view acquisition combined with iterative regularization, hybrid 2D/3D imaging, or carefully validated super-resolution methods. These options should be chosen jointly, because acquisition and reconstruction are coupled parts of the same design problem.

In conventional microfocus tubes the cathode voltage is chosen to balance contrast and flux: lower voltages improve absorption contrast for low-Z phases (consisting of elements with low atomic number) such as polymer electrolyte but decrease photon output and thus temporal resolution. Reiter *et al* [14] showed that adjusting the spectrum to give a minimum transmission of $\sim$14% maximizes CNR, in agreement with non-destructive testing standards EN 16 016–2 (10%–20%) and ISO 15 708–2 ($\sim$14%). Emerging digital x-ray sources based on carbon-nanotube field-emission cathodes relax this trade-off by providing high peak brightness in short, electronically gated pulses, allowing contrast-optimized low-kV operation while keeping the average dose low and eliminating the thermal inertia of filament-driven

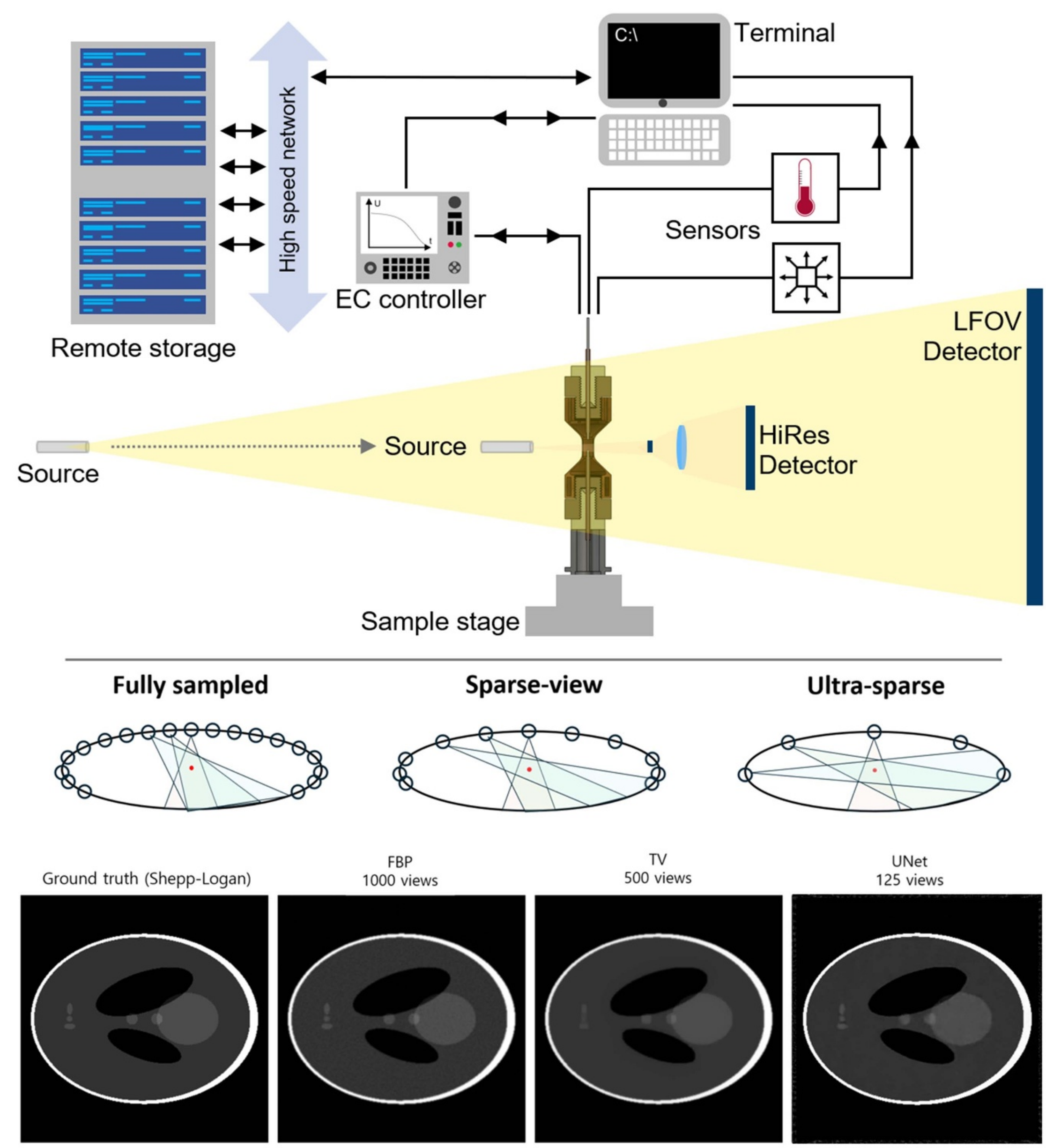

Figure 1. High-level overview of operando laboratory XCT for battery research (top) and illustration of acquisition strategies (bottom). The schematic illustrates key components: x-ray source, rotating sample stage with an electrochemical cell connected to a controller (potentiostat) and detector(s) for capturing projections. Note that two acquisition modes are depicted, one for large field of view imaging and the other for imaging with optical magnification (HiRes). The acquisition strategies at the bottom demonstrate the increasing complexity of reconstruction techniques allowing to resolve the same details despite the reduced projection space.

tubes [15]. Their lack of filament warm-up simplifies adaptation to *in-operando* environments and provides higher temporal resolution without increasing x-ray dose.

The minimum projections needed for analytical reconstruction can be estimated using a Nyquist-based relation Nproj $\approx \pi N_{\mathrm{eff}}/2$, where N_{eff} denotes the effective projected object width on the detector [5, 16]. This estimate should be interpreted as an empirical lower bound and depends on imaging geometry, including magnification, cone angle, and the ratio between object size and field of view. It should therefore be distinguished from sparse-view designs that intentionally use fewer projections and instead rely on iterative or learned reconstruction methods.

Spatial resolution captures phenomena but trades off with total time of experiment and temporal resolution. For example, in lithium plating [13], one can consider a 6 mm diameter sample with lithium on one side, plating on the other at 100 μA cm^{-2}. Using Faraday's law for homogeneous deposition, thickness of plated lithium can be defined as $h = \frac{j\cdot t\cdot M}{n\cdot F\cdot \rho}$, where t is the plating time, j is the current density, n is the number of involved electrons, F is the Faraday constant, ρ is the density and M is the molar mass. Assuming $j = 0.1$ mA cm^{-2}, $M = 6.94$ g mol^{-1} (Li), $n = 1$, F = 96 485 C mol^{-1},

$\rho = 0.534$ g cm^{-3}, it takes approximately 6.2 h to plate a 3 μm thick lithium layer (visible at 3 μm resolution). With $\sim$2 h scans between steps, each cycle takes approximately 8.2 h. Therefore, to deposit 100 μm of lithium we need $\sim$33 steps, $\sim$270 h $\approx$ 11 d. This simple estimate highlights why acquisition-efficient strategies, as depicted in figure 1, are often indispensable for laboratory XCT systems. High-speed approaches such as sparse-view or ultrasparse tomography for 4D imaging [7] and machine-learning-based super-resolution of laboratory CT data [10], together with other optimization routes [17] can substantially ease the resolution–time trade-off by reducing the number of required projections or enabling shorter, lower-magnification scans at comparable effective resolution. Another approach, for homogeneous materials, is using 2D images (radiograms) to extrapolate the 2D attenuation maps to 3D growth rate directly from Beer-Lambert law [2].

In some cases, when interfaces characterized by low contrast are of interest, e.g. lithium vs. polymer electrolyte, it is desirable to enhance the interface by propagation-based phase contrast. Theoretical details with practical values for Xradia scanners can be found in [18]. It is important to remember however that phase contrast geometry, due to large source-detector distance, impacts flux and temporal resolution.

Custom cells enable low source voltage and/or good temporal resolution, especially for lithium systems requiring liquid/gas tightness. As a rule of thumb, polyether ether ketone (PEEK) coated with a thin layer of aluminum offers chemical resistance and low x-ray absorption [13]. The design details of the PEEK cell, including schematics and discussion on material selection can be found in Weckelmann *et al* [13]. 3D-printed cells fabricated using a cheaper and more accessible stereolithographic (SLA) process, have also been reported as suitable for *in-operando* XCT [2].

3. Experiment

Before starting the actual *in-operando* experiment, pristine *in situ* or *ex situ* scans (or both) should be performed. These scans capture the initial state of the system and allow testing of optimal imaging settings (exposure, number of projections, etc.). They also reveal potential issues with the sample, such as faulty synthesis or mishandling that may cause mechanical damage to its components (e.g. cracks). Only after confirming the mechanical integrity of the sample can the electrochemical protocol be executed.

Synchronization between imaging and electrochemistry is likely the most challenging aspect of an *in-operando* laboratory XCT experiment. Some commercial laboratory XCT platforms, including the Zeiss Xradia systems used in the examples discussed here, provide user-accessible scripting interfaces such as Python APIs for programmatic control of scan acquisition, recipe modification, and instrument hardware. Such interfaces are particularly useful for multi-day in-operando experiments, where manual triggering of imaging protocols is impractical. With proper scripting, complex imaging protocols can be implemented, including multiple modalities (2D/3D), regions of interest (ROIs, e.g. separate images for electrolyte and electrodes), and magnifications (overview scans combined with high-resolution imaging). An example is Dzięcioł *et al* [2], where overview scans are interleaved with fast radiography and high-resolution pristine and post-mortem tomography. The provided pseudocode and Python scripts can serve as useful templates for setting up and controlling similar experiments. Note that continuous radiography requires the incorporation of additional reference scans (flat-field) to correct for beam fluctuations, particularly if the x-ray tube voltage has changed in the meantime.

If detailed evolution of morphology is required, multiple scans after short deposition steps can be easily implemented, as demonstrated by Dzięcioł *et al* [3]. In that study, a single discharge step of a commercial zinc-air battery was calibrated to allow assessment of very subtle changes in the morphology of individual zinc particles. This approach, however, resulted in a long-term experiment (>10 d).

Very short 3D scans were enabled by custom cell design in Weckelmann *et al* [13]. There, the protocol consisted of continuous acquisition of radiographs (every 5 min) while potential was applied, followed by $\sim$2-h tomography during open-circuit voltage after each deposition step.

For seamless execution (and design) of the *in-operando* protocol on a laboratory scanner, open-source toolboxes created for specific combination of hardware components, can be used. For example, the Python toolbox developed by Dzięcioł *et al* [3] enables graphical design of imaging sequences, where tomography can be triggered by the falling edge of a control signal from the potentiostat (i.e. when applied current drops to zero). The provided imaging sequence, acquisition parameters and Python source code can be used directly to set up the experiment on zinc coin cells with Xradia systems. With minor modifications, it can be tailored to work with different types of cells and chemistries, as presented by Weckelmann *et al* [13]. Unfortunately, the handling of additional sensors must currently be programmed separately, as no comprehensive software solution yet exists to integrate data from multiple sensors.

During execution of the imaging and electrochemical protocols, the acquired data must be monitored continuously to detect any technical issues with the protocol itself or premature sample failure. For example, sample drift may require correction of the field of view. Conversely, a fast-propagating crack can be mitigated by reducing the applied load or better assessed by increasing the sampling rate (shorter deposition steps). In cases involving liquid electrolytes, inspection of low-resolution overview scans can reveal excessive evaporation or leakage due to cell disintegration or natural permeation. When moving to different ROI or changing lens (zoom-in scan), eventual collision with imaging components needs to be addressed.

Finally, once the experiment is complete, detailed post-mortem *in situ* and/or *ex situ* scans should not be omitted.

4. Data

Once the experiment is concluded, the acquired data must be processed. For fully sampled, quasi-static experiments, standard FBP or FDK reconstruction implemented in the scanner software is typically sufficient. However, *in-operando* measurements often rely on strongly undersampled or non-standard geometries to reach the required temporal resolution. In these cases, iterative, regularized algorithms become indispensable. Using open-source toolboxes such as CIL [9] interfaced with ASTRA [19], users can perform cone-beam reconstructions with [8] TV or other sparsity-promoting priors, which efficiently suppress streak artifacts arising from sparse angular sampling. In practice, the regularization strength should be tuned using simple phantoms or representative regions of interest, balancing noise suppression and preservation of fine interfacial features such as thin dendrites. Note that over-regularization may smooth rough interfaces, suppress thin dendrites or small pores, and bias diameters upward, whereas under-regularization may leave residual streaks or aliasing patterns that mimic real structures. These failure modes are especially pronounced for metal electrodes under ultra-sparse angular sampling and should be assessed before quantitative interpretation.

In genuine 4D experiments, independently reconstructing each time point can cause temporal inconsistency and excess noise. Dynamic reconstruction methods, which link time points using temporal TV or low-rank plus sparse models, help maintain smooth bulk morphology and permit local abrupt changes. Though more computationally intensive, these approaches use limited projections more efficiently and are especially useful for ultrasparse-view protocols.

Increasing temporal resolution by lowering magnification or exposure time can lead to loss of detail and higher noise in tomograms. Deep learning methods, such as super-resolution and denoising with CNNs (2D or 3D U-Net, residual CNN), help restore resolution from low-quality data by mapping them to high-quality reference scans from synchrotron XCT or high-magnification laboratory scans [10, 20].

These methods enhance visual interpretability and support segmentation but should be applied cautiously. Network outputs reflect inferred morphologies and may contain artifacts or training biases. Therefore, one should use deep-learning-enhanced data mainly for qualitative analysis or pre-processing and always validate key quantitative results with conventional reconstructions when possible.

After reconstruction, data reduction should be performed, for example, by cropping the background and converting to 8-bit format. This can reduce required storage by up to an order of magnitude and significantly accelerate further processing. The acquired tomograms must then be aligned using rigid registration to compensate for inevitable sample drift in long-term experiments. The same applies to radiograms; for instance, Dzięcioł *et al* [2] applied phase correlation for sub-pixel alignment of consecutive radiograms to accurately estimate changes in electrode thickness during active material deposition. In that case, a custom MATLAB script was used, but both commercial (e.g. Dragonfly, Avizo) and free (e.g. ImageJ/Fiji [21]) alternatives are available.

In aqueous systems with pronounced gas evolution, bubble nucleation, growth, and migration can introduce local non-rigid deformations that are not well described by global rigid registration. In such cases, gas-rich regions should be masked before registration or excluded from quantitative analysis, and segmentation consistency should be checked across time points to avoid misclassifying mobile bubbles as pores, cracks, or pitting features. Where possible, control experiments at matched cumulative dose under open-circuit conditions can help distinguish irradiation-induced gas generation from electrochemically driven morphology changes.

Structures of interest, such as dendrites, particles, and pores are best delineated using thresholding when possible, as it is efficient in terms of resources and time. This requires normalization, i.e. adjusting to background intensity, for consistency across time points. In cases where interfaces are unclear due to resolution, contrast, or noise issues, advanced approaches like Trainable Weka Segmentation (ImageJ/Fiji) or deep learning-based U-Net models may be necessary, as demonstrated in recent studies [3, 22].

After segmentation, morphological descriptors—including surface roughness, area, equivalent diameter, orientation, and sphericity—can be computed. Quantitative analysis involves tracking changes in these descriptors over time and correlating them with electrochemical data to uncover mechanisms or validate models, and can suggest improvements in electrode morphology [3]. Visualization and analysis are typically performed using custom scripts or software such as ImageJ/Fiji, Dragonfly, or Avizo.

5. Practical considerations

When optimizing acquisition parameters for an *in-operando* protocol, various imaging artifacts may be encountered. For example, high-energy flux applied to strongly attenuating materials can cause beam hardening, resulting in cupping effects [23] and/or streak artifacts between highly absorbing elements [23]. These cannot always be fully corrected by post-processing; therefore, beam filtering or lowering the tube voltage should be considered. Ring artifacts, caused by miscalibrated detector elements, are typically corrected using flat-field reference images [23]. If this is insufficient, a stronger filter or a secondary flat-field acquisition with a stronger filter should be used.

In addition, limited-angle trajectories (e.g. laminography or restricted rotation in bulky *in-operando* cells) can introduce characteristic elongation and streaking artifacts, while aggressive sparse-view sampling may lead to aliasing or temporal blurring if regularization is insufficient; both effects should be assessed on simple phantoms before applying a given protocol to real cells. Despite optimized acquisition times, motion artifacts may still appear. These indicate poor sample holder fixation, thermal expansion, incorrect prediction of morphology evolution (too rapid), or beam-induced damage. In the case of the latter, the only solution is to reduce the dose—by applying a filter, shortening exposure, or reducing source power. The same applies to thermal expansion if pre-heating the sample with the beam prior to imaging is not feasible due to time constraints. Sparse sampling and super-resolution strategies, as discussed in previous sections, can also be employed to reduce dose.

Gas evolution (e.g. hydrogen in zinc systems with liquid electrolyte) can generate bubbles that affect tomograms and radiograms and, more critically, pose explosion risks. Allowing the gas bubbles to escape, e.g. by perforated top will reduce the reconstruction artifacts (see Dzięcioł *et al* [2]) but requires extra precaution. For safety, the concentration of volatile and explosive gases should be calculated theoretically using Faraday's law (e.g. H_2 concentration kept below 4%) and monitored if possible. For lithium systems, glovebox assembly prevents oxidation artifacts.

In addition to hardware-related artifacts, reconstruction and post-processing algorithms can introduce systematic errors. Over-regularized iterative reconstructions may smooth interfaces, suppressing thin dendrites or small pores that are crucial for mechanistic interpretation. Conversely, insufficient regularization can leave residual streaks or aliasing patterns that mimic real features. Users are therefore advised to validate reconstruction parameters on simple phantoms or early *in-operando* time points where the morphology is known. Similarly, learning-based super-resolution and segmentation models can introduce hallucinated features or subtle biases if trained on a limited or non-representative dataset [24]. To mitigate this, temporal leakage between training and test data must be avoided, and key quantitative conclusions should be cross-checked using minimally processed reconstructions and, where available, independent measurements.

Since *in-operando* measurements—especially with optimized acquisition (low exposure enabling high sampling rates of the electrochemical protocol)—may generate hundreds of gigabytes of data, a dedicated computing node with high-speed RAID storage is highly recommended.

As a practical planning aid, table 1 summarizes typical parameter considerations for representative battery XCT scenarios. The values are not intended as universal prescriptions, but as starting points that should be adjusted according to scanner flux, field of view, sample attenuation, electrochemical rate, and the required quantitative endpoint.

Note that most important steps necessary to design and implement *in-operando* imaging experiment are summarized, together with relevant references, in the figure 2 as a 'cheat-sheet'. Additionally, in table 2, the common *in-operando* XCT issues are listed together with mitigation strategies.

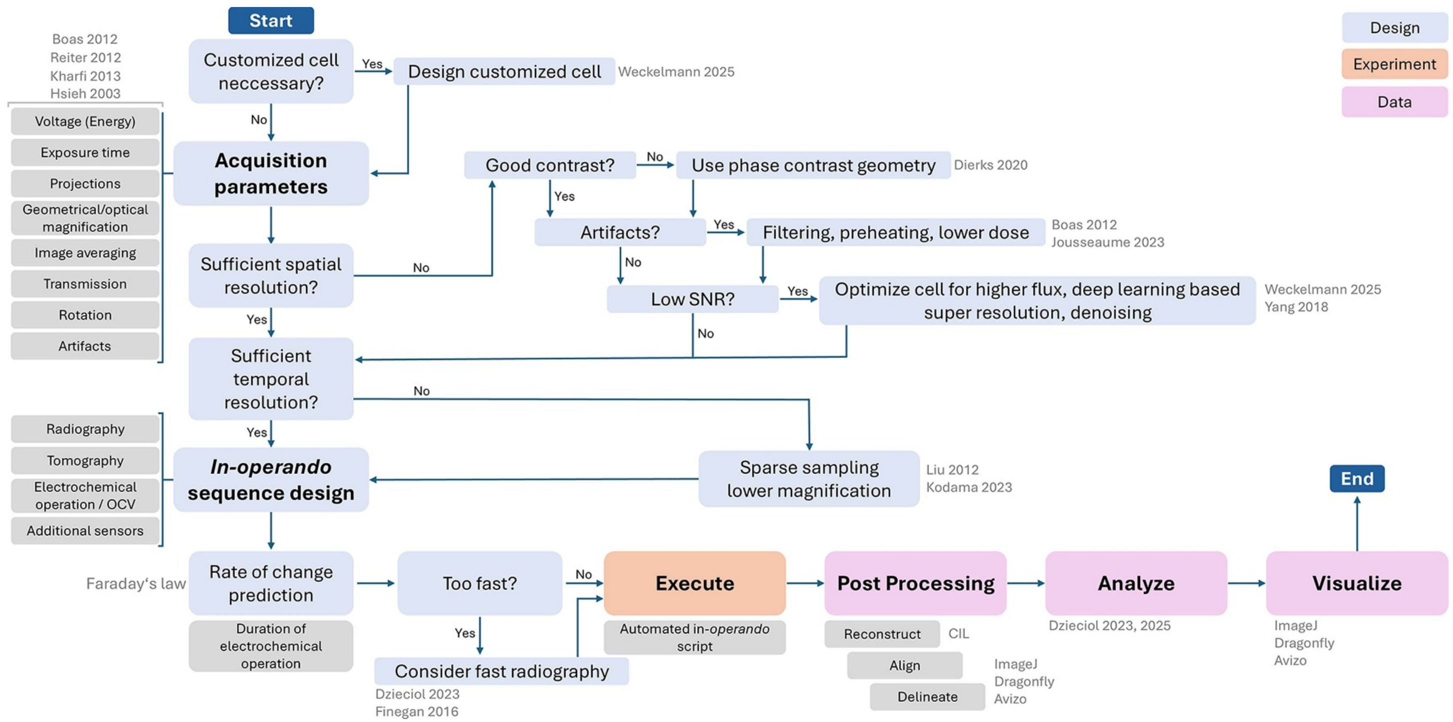

Figure 2. Cheat-sheet for design and execution of *in-operando* XCT study.

Table 1. Scenario-specific parameter considerations for *in-operando* laboratory XCT of battery systems.

Target phenomenon	Required spatial resolution	Expected time scale	Suggested imaging mode	Exposure/projection considerations	Key artifacts to monitor
Li plating and dendrite growth	sub-μm	minutes to days	intermittent high-resolution 3D in the sealed cell, phase contrast if needed	short deposition steps, validation against conventional reconstruction	low contrast, segmentation bias, thin-feature loss, oxidation artifacts
Zn anode morphology evolution	sub-μm to few μm	minutes to days	hybrid 2D/3D	balance projection number and scan time, sparse-view possible for faster dynamics	gas bubbles, drift, segmentation instability, sparse-view streaks
Gas bubble evolution in aqueous cells	few μm to tens of μm	seconds to hours	fast radiography, preferably with phase contrast	short exposure, high sampling rate	non-rigid deformation, bubble migration, beam induced gas evolution
Electrode swelling or cracking	few μm to tens of μm	minutes to hours	hybrid 2D/3D	moderate projection number, maintain sufficient CNR for boundaries	motion artifacts, registration errors, beam hardening

Table 2. Common problems and proposed solutions. Note that for beam hardening and ring artifacts it was assumed that software corrections, normally applied by device's reconstruction software, were not sufficient.

Problem	Solution (s)
Beam hardening induced cupping and or streak artifacts	Beam filtering, lower voltage
Ring artifacts	Beam filtering, secondary reference
Streaking/aliasing in sparse view data	Stronger priors, more projections, validation on phantom, stronger regularization
Missing details in sparse view data	Stronger priors, more projections, validation on phantom, weaker regularization
Drift across time points	Registration
Motion artifacts	Improve sample fixation, pre-heat (thermal expansion), lower dose (beam damage), shorter exposure
High noise level	Longer exposure, more averages, denoising
Unstable segmentation across time points	Intensity normalization, masking moving gas regions, supervised segmentation

6. Summary

This tutorial covers key aspects of *in-operando* laboratory XCT experiments, such as selecting appropriate hardware and reconstruction technique, optimizing protocols, minimizing artifacts, and managing data, along with multiple minor tips. Relevant references are included to support the material discussed. The authors hope this guidance will make *in-operando* imaging more accessible at research institutions, even though laboratory devices offer less flux than synchrotron sources. The technique still demands custom cells and careful tuning due to lower throughput. Nevertheless, recent progress in sparse sampling and super-resolution methods could make it a powerful tool for non-destructive observation of battery dynamics, connecting electrochemical processes with structural information.

7. Highly recommended/further reading

Reader is advised to look into books of Hsieh [5] and Kak & Slaney [6] for more details on computed tomography. Application to material science is covered by Banhart [25], while comprehensive review on optimizations for high speed imaging was done by Zwanenburg *et al* [17]. Practical applications to battery research are provided by Dzieciol *et al* [2, 3] and Weckelmann *et al* [13]. The latter is especially recommended for more details on cell design aspects including material selection, sealing and sensor integration. Beyond the battery research the *in-operando* XCT is reported e.g. to study electrolysis [26] or CO_2 reduction [27].

Acknowledgment

The authors acknowledge the financial support from the Federal Ministry of Research, Technology and Aeronautics (BMFTR) within the project 'iNEW2.0—Inkubator Nachhaltige Elektrochemische Wertschöpfungsketten' Project No. 03SF0627A and within the project 'US-German Cooperation on Energy Storage' under the funding program 'LiSI-2-Lithium-Solid-Electrolyte Interfaces' Project No. 13XP0509A.

This research was supported by the National Research Council of Science & Technology (NST) Grant by the Korea government (MSIT) (No. CAP25021-000).

Data availability statement

No new data were created or analysed in this study.

Author contributions

Krzysztof Dzieciol 0009-0009-6296-1513
Conceptualization (equal), Data curation (equal), Formal analysis (equal), Investigation (equal), Methodology (equal), Project administration (equal), Supervision (equal), Validation (equal), Visualization (equal), Writing – original draft (equal), Writing – review & editing (equal)

Sunghoon Choi 0000-0003-1714-5233
Conceptualization (equal), Data curation (equal), Formal analysis (equal), Investigation (equal), Methodology (equal), Project administration (equal), Supervision (equal), Validation (equal), Visualization (equal), Writing – original draft (equal), Writing – review & editing (equal)

Luca Weckelmann 0009-0001-6552-5583
Methodology (equal), Validation (equal), Visualization (equal), Writing – original draft (equal), Writing – review & editing (equal)

Rebecca Erkes 0009-0008-9812-8059
Investigation (supporting), Methodology (supporting), Validation (equal), Writing – review & editing (supporting)

Rüdiger-A Eichel
Project administration (equal), Resources (equal), Supervision (equal), Writing – review & editing (supporting)

Florian Hausen 0000-0001-5712-6761
Conceptualization (equal), Methodology (equal), Project administration (equal), Supervision (equal), Writing – review & editing (supporting)

References

[1] Black A P *et al* 2023 Synchrotron radiation based operando characterization of battery materials *Chem. Sci.* **14** 1641–65
[2] Dzięcioł K, Durmus Y E, Tempel H, Kungl H, Bauer A and Eichel R-A 2023 Laboratory x-ray computed tomography imaging protocol allowing the operando investigation of electrode material evolution in various environments *iScience* **26** 107097
[3] Dzięcioł K, Durmus Y E, Im E, Tempel H, Hausen F and Eichel R-A 2025 Operando XCT with fine sampling of discharge process provides new insights into anode's morphology evolution in a commercial zinc-air battery *Methods Microsc.* **2** 317–28
[4] Huang Y *et al* 2023 Detecting lithium plating dynamics in a solid-state battery with operando x-ray computed tomography using machine learning *Npj Comput. Mater.* **9** 93
[5] Hsieh J 2003 *Computed Tomography* (SPIE Press)
[6] Kak A C and Slaney M 1988 *Principles of Computerized Tomographic Imaging* (IEEE Press)
[7] Zheng Y and Hatzell K B 2023 Ultrasparse View x-ray computed tomography for 4D Imaging *ACS Appl. Mater. Interfaces* **15** 35024–33
[8] Liu Y, Ma J, Fan Y and Liang Z 2012 Adaptive-weighted total variation minimization for sparse data toward low-dose x-ray computed tomography image reconstruction *Phys. Med. Biol.* **57** 7923

[9] Jørgensen J S *et al* 2021 Core imaging library—Part I: a versatile python framework for tomographic imaging *Phil. Trans. R. Soc. Math. Phys. Eng. Sci.* **379** 20200192
[10] Kodama M, Takeuchi A, Uesugi M and Hirai S 2023 Machine learning super-resolution of laboratory CT images in all-solid-state batteries using synchrotron radiation CT as training data *Energy AI* **14** 100305
[11] Finegan D P *et al* 2015 In-operando high-speed tomography of lithium-ion batteries during thermal runaway *Nat. Commun.* **6** 6924
[12] Du W *et al* 2025 x-ray computed laminography: a brief review of mechanisms, reconstruction, applications and perspectives *Mater. Today* **86** 267–81
[13] Weckelmann L *et al* 2025 A novel pressurized operando battery cell for laboratory x-ray computed tomography *Methods Microsc.* **2** 417–30
[14] Reiter M *et al* 2012 Evaluation of transmission based image quality optimisation for x-ray computed tomography: conference on Industrial Computed Tomography 2012 (iCT2012) *Conf. Ind. Comput. Tomogr. ICT2012* pp. 241–50
[15] Lee Y Z, Burk L, Wang K, Cao G, Lu J and Zhou O 2011 Carbon nanotube based x-ray sources: applications in pre-clinical and medical imaging *Nucl. Instrum. Methods Phys. Res. Sect. Accel. Spectrometers Detect. Assoc. Equip.* **648** S281–S3
[16] Kharfi F 2013 Mathematics and physics of computed tomography (CT): demonstrations and practical examples *Imaging and Radioanalytical Techniques in Interdisciplinary Research—Fundamentals and Cutting Edge Applications* (IntechOpen) (https://doi.org/10.5772/52351)
[17] Zwanenburg E A, Williams M A and Warnett J M 2021 Review of high-speed imaging with lab-based x-ray computed tomography *Meas. Sci. Technol.* **33** 012003
[18] Dierks H and Wallentin J 2020 Experimental optimization of x-ray propagation-based phase contrast imaging geometry *Opt. Express* **28** 29562–75
[19] van Aarle W *et al* 2016 Fast and flexible x-ray tomography using the ASTRA toolbox *Opt. Express* **24** 25129–47
[20] Yang X *et al* 2018 Low-dose x-ray tomography through a deep convolutional neural network *Sci. Rep.* **8** 2575
[21] Schindelin J *et al* 2012 Fiji: an open-source platform for biological-image analysis *Nat. Methods* **9** 676–82
[22] Müller S *et al* 2021 Deep learning-based segmentation of lithium-ion battery microstructures enhanced by artificially generated electrodes *Nat. Commun.* **12** 6205
[23] Boas F E and Fleischmann D 2012 CT artifacts: causes and reduction techniques *Imaging Med.* **4** 229–40
[24] Bhadra S, Kelkar V A, Brooks F J and Anastasio M A 2021 On hallucinations in tomographic image reconstruction *IEEE Trans. Med. Imaging* **40** 3249–60
[25] Banhart J 2008 *Advanced Tomography Methods in Materials Research and Engineering* (Oxford University Press)
[26] Leonard E *et al* 2020 Interfacial analysis of a PEM electrolyzer using x-ray computed tomography *Sustain. Energy Fuels* **4** 921–31
[27] Lee S A *et al* 2025 Visualizing degradation mechanisms in a gas-fed CO2 reduction cell via operando x-ray tomography *EES Catal.* **3** 1302–14